JOURNAL OF MATERIALS SCIENCE 29 (1994) 5801–5807

Densification process of α′-sialon ceramics

K. WATARI, T. NAGAOKA, S. KANZAKI
National Industrial Research Institute of Nagoya, Kita-ku, Nagoya 462, Japan

The liquid-phase sintering process of α′-sialon ceramics has been investigated by high-temperature dilatometry and microstructural observation. In addition, isothermal shrinkage measurements have been performed to examine the densification kinetic parameter. It has been confirmed that densification kinetic parameters in the solution-reprecipitation stage are much larger than the rate exponent predicted for the classic liquid-phase sintering model, and are slightly smaller than that for the viscous flow process. Rapid shrinkage was observed in the solution–reprecipitation stage from the results of shrinkage rate, and corresponds to pore elimination by particle rearrangement and cooperative flow of particle/liquid mixture. These processes provide the major contribution to shrinkage. In addition, the liquid flow process occurs when the silica content in the raw powder increases, but it is retarded due to the formation of α′-sialon. It is anticipated that particle rearrangement and cooperative flow, as well as liquid-flow processes, take place in the solution-reprecipitation stage of sintering of Si_3N_4-based materials, and cause a large amount of shrinkage.

1. Introduction

Si_3N_4 ceramics have two polytypes, α and β. The solid solutions in β-Si_3N_4, which are usually called β′-sialon, are formed by substituting equal amounts of aluminium and oxygen for silicon and nitrogen, respectively, and are expressed by the general formula, $Si_{6-z}Al_zO_zN_{8-z}$, where $0 < z < 4.2$ [1, 2]. On the other hand, α′-sialon ceramics, which are the solid solutions with α - structure, are obtained by a substitution of similar elements to β′-sialon, and also can accommodate some metal cations into the two large interstices of the unit cell. They can be described by a general formula of the type $M_x(Si,Al)_{12}(N,O)_{16}$, where M is calcium, lithium, magnesium and yttrium or lanthanide metals except lanthanum and cesium, and $0.3 < x < 2.0$ [3–5].

It is reported that the formation and densification of α′-sialon proceed through the dissolution of Si_3N_4 and AlN into a liquid and reprecipitation, accompanied by the formation of a transient liquid and a solid phase [6]. As the ingredients of the liquid are accommodated into the α-structure during sintering, the viscosity and the amount of liquid phase increases and decreases, respectively [7]. These changes in viscosity and amount of liquid phase will be responsible for the retarding of densification kinetics in the solution–reprecipitation stage. In the present work, the densification process of α′-sialon ceramics has been studied by high-temperature dilatometry and microstructural observation. An investigation of the effect of powder characteristics, e.g. silica content in the raw material, on densification is also reported.

2. Experimental procedures

The starting materials used were commercial Si_3N_4 (Denki Kagaku Kogyo, K.K., Japan), AlN (Tokuyama Soda Co. Ltd, Japan), Y_2O_3 (Hokko Chemicals Co. Ltd, Japan) and SiO_2 (Hokko Chemicals Co. Ltd, Japan) powders. The Si_3N_4 powders were synthesized by direct nitridation of metallic silicon, and their characteristics are summarized in Table I. The AlN powder had oxygen content of 1.1 wt % and a specific surface area of 3.2 $m^2 g^{-1}$. The purity of raw Y_2O_3 and SiO_2 powders was 99.99%.

The chemical compositions of the starting mixtures are presented in Table II. Specimens S, B and C were prepared to explore the effect of powder properties on densification. The nominal compositions of the powder mixture for specimen S, B and C corresponded to $x = 0.5$ in $Y_x(Si, Al)_{12}(N, O)_{16}$. This composition would be a single-phase α′-sialon, according to the phase diagram [4, 5]. Moreover, SiO_2 was added to powder mixture of specimen S, in order to examine the influence of silica content in raw Si_3N_4 powder on the sintering process. The molar ratios of Si_3N_4, AlN and Y_2O_3 in specimens S1 and S2 are the same as in specimen S.

The starting materials were vibrationally milled in methanol for 5 h using an Si_3N_4 pot and balls. The methanol was evaporated at 80 °C in a nitrogen gas, and mixed powders were passed through a 60 mesh sieve. After drying at 120 °C in a vacuum, mixed powders were pressed into rectangular bars (about 10 mm × 10 mm in section and 45 mm in height) and discs (about 14 mm diameter and 8 mm high). Finally, the rectangular bars and discs were cold isostatically pressed (CIPed) under 200 MPa for 60 s. The green density of specimens S, B, C, S1 and S2 was 1904, 1870, 1760, 1830 and 1821 $Kg m^{-3}$, respectively.

For observation of the sintering behaviour, dilatometry was carried out using a high-temperature dilatometer (HPHT-TMA, Rigaku Denki, Co. Ltd, Japan). Detection errors of shrinkage and shrinkage

0022–2461

TABLE I Representative properties of raw Si_3N_4 powder

Powder	Specific surface area (m^2g^{-1})	Oxygen content (wt %)	Carbon content (wt %)	α-phase content (%)
S	12	1.28	0.07	91.6
B	11	0.61	0.13	8.6
C	2.1	0.43	0.15	93.0

TABLE II The composition of the starting mixtures

Specimen	Composition (wt %)			
	Si_3N_4	AlN	Y_2O_3	SiO_2
S	75.47 (powder S)	15.27	9.25	
B	75.47 (powder B)	15.27	9.25	
C	75.47 (powder C)	15.27	9.25	
S1	75.09 (powder S)	15.19	9.20	0.5
S2	74.72 (powder S)	15.12	9.15	1.0

rate were less than 1.8×10^{-2} % and 3.2×10^{-3} % min^{-1}, respectively. Details of the equipment for thermal shrinkage measurement have been described elsewhere [8]. Thermal shrinkage of rectangular bars was measured at temperatures between 1000 and 1950 °C in a nitrogen atmosphere. After thermal shrinkage measurement, specimens were continuously heated for 15 min, and thereafter quenched. Isothermal shrinkage measurement was performed at 1500, 1550 and 1600 °C for 2 h. In all the cases, the heating rate and gas pressure were 10 °C min^{-1} and 1 MPa, respectively.

In order to observe changes in microstructural development and reaction sequence at each sintering temperature, compacted discs were put in a mixture of 50% BN, 37.74% Si_3N_4, 7.64% AlN and 4.62% Y_2O_3 in weight, calcined separately at 1600 °C prior to sintering, and then they were heated in a graphite furnace at temperatures from 1100–1900 °C for 15 min at a heating rate of 10 °C min^{-1} under a nitrogen gas pressure of 1 MPa, followed by quenching.

The bulk density of the sintered specimen was measured by Archimedes' method in distilled water. Relative density was obtained by comparing the measured density with the theoretical density. The theoretical density of α′-sialon was calculated from the amount and density of Si_3N_4, AlN and Y_2O_3, and was estimated to be 3347 Kg m^{-3}. The crystalline phases present were identified by powder X-ray diffraction (RAD-RB, Rigaku Denki, Co. Ltd, Japan) with CuK_α radiation at 40 kV and 100 mA. The relative intensity of the crystalline phases was obtained by comparing the peak intensity of the crystalline phase present to the standard silicon added. The α′-sialon content was calculated from a fractional peak intensity of α′-sialon to the sum of α-Si_3N_4 [(1 0 2) + (2 1 0) reflections] and α′-sialon [(1 0 2) + (2 1 0) reflections]. The microstructure of the fractured surface of specimens was observed by scanning electron microscopy (SEM. T-330AS, Jeol, Japan).

3. Results

Fig. 1 indicates the shrinkage of specimens S, B and C. The shrinkage of specimens S and B proceed with increasing temperature, but an expansion is found at 1700–1800 °C for specimen C. More detailed behaviour of sintering is observed in the shrinkage rate curve of Fig. 2. For specimen S, shrinkage starts at 1120 °C, and the shrinkage rate shows a first maximum at 1250 °C, decreasing slowly until near 1350 °C. At temperatures higher than 1400 °C the shrinkage rate increases rapidly, reaching a second maximum at 1620 °C, followed by an equally rapid decrease through temperature near 1700 °C. Thereafter, the shrinkage rate presents a new increase, showing a third maximum at 1800 °C. In the case of specimen B the shrinkage rate peak is found at temperatures between 1500 and 1700 °C and at temperatures between 1700 and 1900 °C, and the shape of the former peak is very similar to that of the shrinkage rate peak of specimen S at 1500 and 1700 °C. For specimen C, two small peaks are observed at temperatures higher than 1600 °C. The relative density and α′-sialon content of specimens S, B and C after thermal shrinkage measurements are shown in Table III.

The temperature dependence of shrinkage and shrinkage rate for specimens S, S1 and S2 is shown in Figs 3 and 4. The shrinkage rate is characterized by

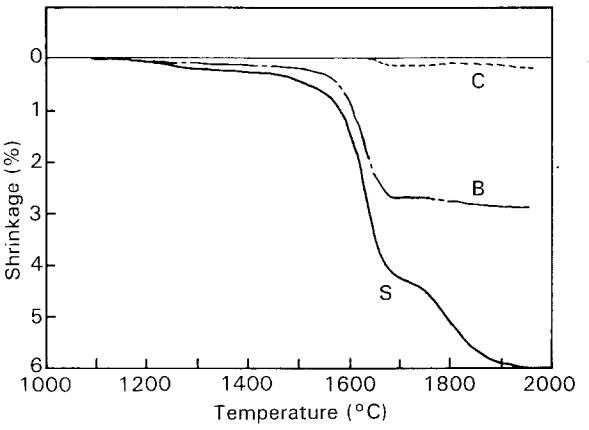

Figure 1 The shrinkage curves of specimens S, B and C. The relative density and α′-sialon content after shrinkage measurement at 195 °C for 15 min are shown in Table III.

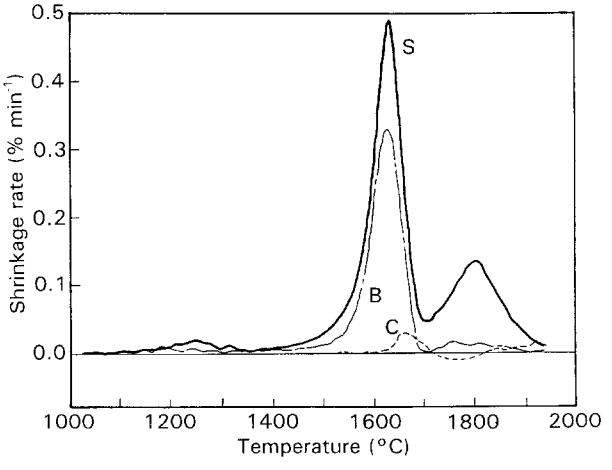

Figure 2 The shrinkage-rate curves of specimens S, B and C.

TABLE III The relative density and α′-sialon content of specimens after shrinkage measurement

Specimen	Sintering condition	Relative density (%) [a]	α′-sialon content (%) [b]
S	1950 °C, 15 min	67.4	100
B	1950 °C, 15 min	60.8	100
C	1950 °C, 15 min	54.1	82
S1	1950 °C, 15 min	83.7	100
S2	1950 °C, 15 min	85.0	100
S	1500 °C, 2 h	62.2	30
S	1550 °C, 2 h	68.4	45
S	1600 °C, 2 h	72.1	75

[a] Theoretical density is estimated as 3350 kg m^{-3}.
[b] Obtained as a fractional peak intensity of α′-sialon to the sum of α-Si_3N_4 [(1 0 2) + (2 1 0) reflections] and α′-sialon [(1 0 2) + (2 1 0) reflections].

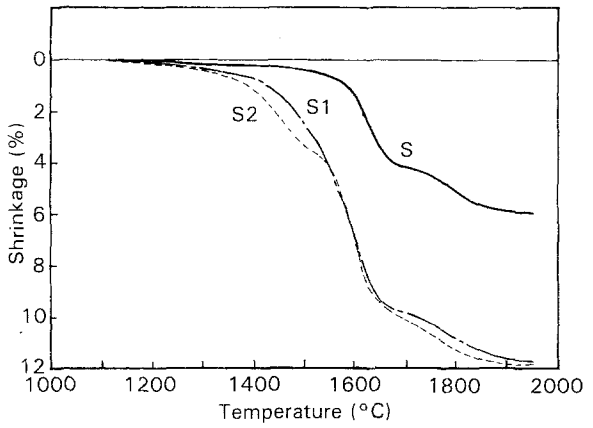

Figure 3 The shrinkage curves of specimens S, S1 and S2. The relative density and α′-sialon content after shrinkage measurements at 1950 °C for 15 min are shown in Table III.

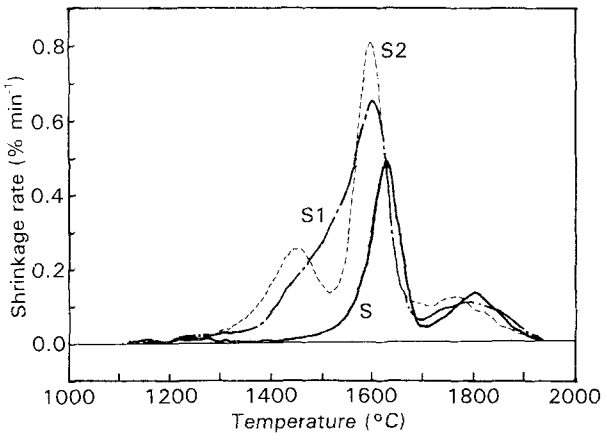

Figure 4 The shrinkage-rate curves of specimens S, S1 and S2.

two maxima at 1600 and 1790 °C for specimen S1 and three maxima at 1450, 1600 and 1780 °C for specimen S2. After the shrinkage measurements at 1950 °C for 5 min, specimen S2 has highest relative density in the present work, as seen in Table III.

The results of isothermal shrinkage of specimen S are shown in Fig. 5. Isothermal shrinkage at 1500 and 1550 °C increases continuously with increasing soaking time, but shrinkage at 1600 °C ceases after 15 min.

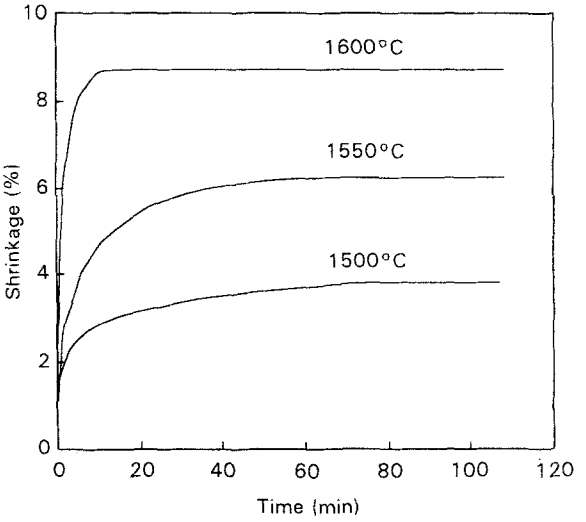

Figure 5 Isothermal shrinkage of specimen S. The relative density and α′-sialon content after isothermal shrinkage measurement for 2 h are indicated in Table III.

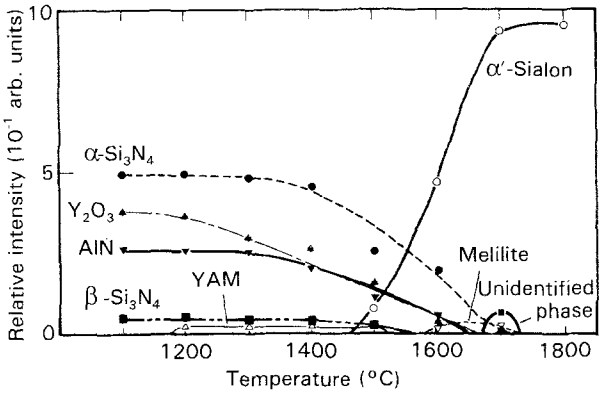

Figure 6 Reaction sequence of the formation of α′-sialon in specimen S fired at 1100–1950 °C for 15 min and quenched. The relative intensity of crystalline phases was obtained by comparing the X-ray peak intensity of the crystalline phase present to the standard silicon (1 1 1).

The relative density and α′-sialon content of specimen S after isothermal shrinkage measurement are also indicated in Table III. With increasing temperature, the relative density and α′-sialon content are augmented.

Fig. 6 shows the reaction sequence of the formation of α′-sialon in specimen S. The amount of raw α-Si_3N_4 and AlN decreases above 1300 °C, and disappears completely at temperatures higher than 1700 °C. The formation of α′-sialon is observed at temperatures higher than 1500 °C, and a rapid increase in its amount is seen at temperatures between 1500 and 1700 °C. The crystalline phases are YAM for specimens sintered at 1200–1500 °C, and melilite for those sintered at 1600 and 1700 °C. An unidentified phase is detected at 1700 °C. Finally, no crystalline phase except α′-sialon is found in the specimen.

Scanning electron micrographs of the fractured surface of discs CIPed and quenched in the temperature range 1400–1900 °C for 15 min are shown in Fig. 7. Irregular-shaped grains, with a wide particle-size distribution, are found in the CIPed specimen (Fig. 7a).

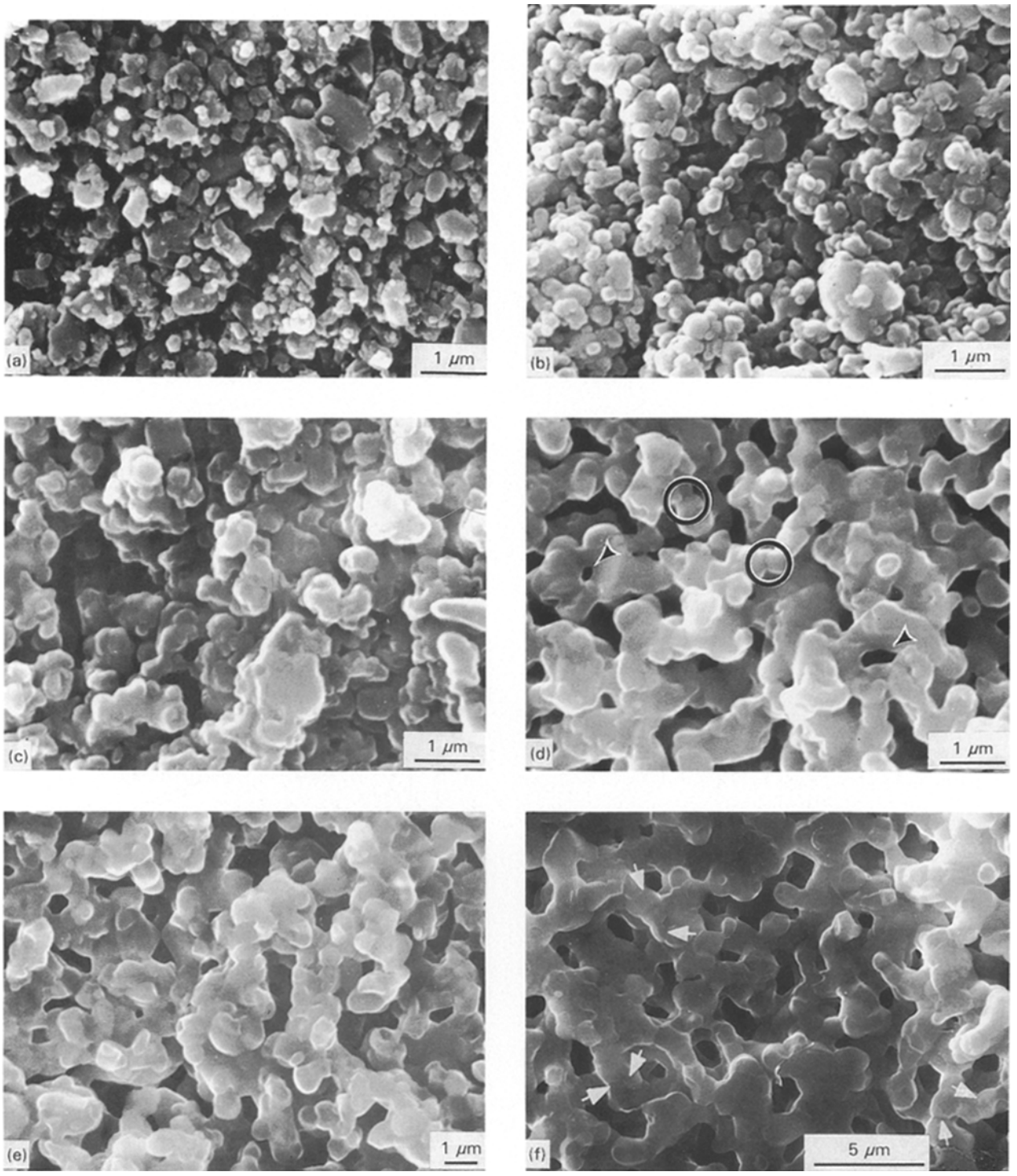

Figure 7 Fractured surface of specimens S (a) CIPed and heated for 15 min, at (b) 1400, (c) 1600, (d) 1700, (e) 1800 and (f) 1900 °C. Small "neck-like region" connecting particles, isolated pores and direct contact of particles are indicated by black circles, black arrows and white arrows, respectively.

After quenching at 1400 °C the grains change to spherical or roundish grains with a smooth surface (Fig. 7b). In the specimen sintered at 1600 °C the particles seem to be covered by a film, and the shape and boundary of particles cannot be found clearly (Fig. 7c). At 1700 °C, the particles are connected to each other by neck-like regions (indicated by black circles), and isolated pores (indicated by black arrows) are also observed (Fig. 7d). With increasing sintering temperature, the agglomerations of particles proceeds (Fig. 7e), and direct contact of particles (indicated by the white arrows) is seen in specimens sintered at 1900 °C (Fig. 7f). Furthermore, the size of pores increases when the temperature is increased (Fig. 7f).

4. Discussion

4.1. Analysis of densification kinetic parameters

It is generally accepted that densification of Si_3N_4 ceramics with an oxide additive and Si_3N_4 solid solutions proceeds via a liquid-phase sintering, which

consists of three distinct stages, (I) particle rearrangement, (II) solution-reprecipitation and (III) coalescence of grains [9]. These sintering stages are usually plotted as the logarithm of linear shrinkage versus the logarithm of time. The kinetic equation for isothermal shrinkage is generally expressed by

$$\Delta L/L_0 = \kappa r^{-m} t^{-n} \quad (1)$$

where $\Delta L = L_0 - L$, L_0 and L are the lengths of the specimen at times t_0 and t, respectively, and κ is a proportional constant, r the grain size, and m and n are constant. The values of m and n depend on the shape of the particle and on the rate-controlling process. In the particle-rearrangement process, $n = 1 + y$. This process at the initial step corresponds to a viscous flow ($n = 1$), and in progress, causes further particle migration [9]. In the usual treatment, $n = 1.1 - 1.6$ [10]. In the solution–reprecipitation stage, $n = 0.5$ or 0.33 for a reaction- or diffusion-controlled mechanism, respectively, in the presence of roundish particles [9]. The roundish particles observed at 1400 and 1600 °C show that densification of specimen A can be kinetically analysed according to Kingery's model.

The results of isothermal shrinkage at 1500, 1550 and 1600 °C, as indicated in Fig. 5, are plotted on a logarithmical scale, and are shown in Fig. 8. The rate exponent, n, on the initial slope was 0.81 for 1500 and 1550 °C, and 0.82 for 1600 °C. These values are slightly smaller than the value predicted for a viscous flow process, and are much larger than that predicted for the solution–reprecipitation stage. The reason why the sintering stage does not follow the above classic model is because, on the basis of Kingery's model, it is assumed that each process takes place separately [9]. However, in the case of sintering of most ceramics, several processes occur simultaneously.

Our previous work [11] reported that densification of coarse AlN powder in the initial stage progresses by concurrent particle rearrangement and solution–reprecipitation processes, resulting in n values lower than the theoretical one for particle rearrangement. Suttor and Fischman [12] discussed the densification process on the basis of sintering kinetic parameters for the Si_3N_4–Al_2O_3–Y_2O_3 system, and reported a larger-than-predicted value for the solution–reprecipitation stage. They have concluded that densification in the second stage proceeds by several additional solution–reprecipitation processes, such as Ostwald ripening with shape accommodation, particle disintegration, liquid flow or cooperative flow of particle/liquid mixture. From the present results of the densification kinetic parameters, it is considered that a particle rearrangement process, liquid-flow process, cooperative-flow process of the particle/liquid mixture and so on, contribute to the shrinkage in the solution–reprecipitation stage for α′-sialon. More details of the densification process are discussed on the basis of the results of shrinkage rate and scanning electron micrographs of the fractured surfaces.

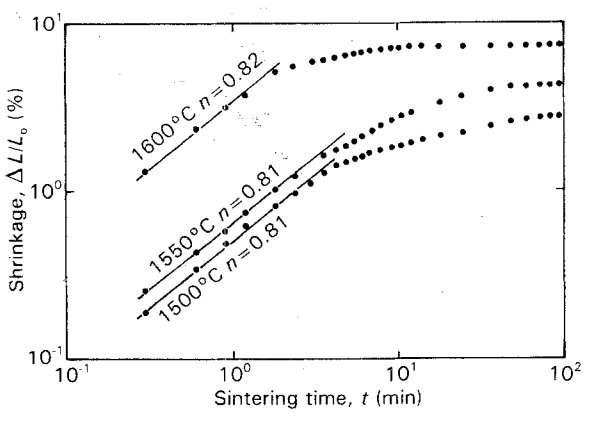

Figure 8 Plots of linear shrinkage versus time.

4.2. Analysis of shrinkage-rate curve

From the results of shrinkage rate, the sintering process of specimen S can be roughly divided into three temperature range: (i) 1120–1350 °C, (ii) 1350–1700 °C and (iii) above 1700 °C. The shrinkage-rate peak in the 1120–1350 °C interval is attributed to an initial particle rearrangement process, because this temperature range is equal to the lowest eutectic temperature in the Si_3N_4–Y_2O_3–Al_2O_3 system containing impurities [13]. However, as shown in Fig. 1, the amount of shrinkage achieved through the primary rearrangement process is less than 0.3%, one of the reasons being the characteristics of the raw powders. As shown in Fig. 7a, the microstructure of the CIPed sample consists of irregular shape grains, resulting in increased resistance to particle migration. Also the viscosity of liquid in this temperature range is considered to be too high to allow migration of the particles. Therefore, the densification fraction, due to primary particle rearrangement, is very small.

The temperature range higher than 1350 °C corresponds to the solution–reprecipitation stage. During this stage grain growth occurs through the dissolution of small particles, diffusion of material in the liquid and reprecipitation on large particles [9]. As shown in Fig. 7b, roundish grains with a smooth surface are appeared, implying that irregular parts in the grains and small particles are selectively dissolved by a liquid. This evidence is also supported by the decrease in the amount of Si_3N_4 and AlN above 1400 °C, as shown in Fig. 6.

A rapid increase and decrease of shrinkage rate are observed at 1500–1700 °C. A similar shrinkage-rate peak is also seen in specimen B. It is interpreted that in the case of liquid–phase sintering, the sintering phenomenon corresponds to pore elimination by particle rearrangement and cooperative flow of the particle/liquid mixture, because the particle migration to fill up the interstice and large pores proceeds rapidly. In a previous work [11] we have investigated the densification process of roundish AlN powders with various specific surface areas by high-temperature dilatometry, and we found the shrinkage-rate peak to correspond to the rearrangement process and cooperative flow process of the particle/liquid mixture in the sintering of fine AlN powders. The shape of this peak was extremely sharp. Its shape resembles that of the peak observed at 1500–1700 °C in Fig. 2, so the

shrinkage in this temperature range might be attributed to a particle-rearrangement process and cooperative-flow process of the particles/liquid mixture.

Evidence of pore elimination by particle migration can be explained from the microstructural features. The presence of indistinct boundaries between the particles, as seen in Fig. 7c, indicates that the particles are covered with enough liquid during the sintering. It is easy to move the roundish particles towards to the large pores, owing to the decrease in friction between the particles. Previously, Kingery [14], Petzow and Kaysser [15, 16] pointed out that in the sintering of small particles in the presence of a large amount of liquid, large pores are eliminated by a cooperative flow of particle/liquid, comparable to viscous flow. Also, Yoon and co-workers [17, 18] pointed out that pore elimination by viscous flow in the presence of a wetting liquid or particle/liquid mixture is possible. Considering that particles are covered with sufficient liquid, pores can be eliminated by particle migration.

Furthermore, the presence of a neck connecting the particles and small isolated pores, as seen in Fig. 7d implies that a liquid bridge forms between the particles, which causes particle movement by capillary forces of the liquid. Hence, densification at 1500–1700 °C is related to the elimination of pores, which is due to particle rearrangement and cooperative flow of the particles/liquid mixture.

It has been found by Petzow and Kaysser [15, 16] that in the sintering of several metals and oxide ceramics, the reduction in pore volume occurs by particle migration in the solution–reprecipitation stage. This process is called "secondary particle rearrangement" to distinguish it from the primary rearrangement process of the initial stage. In this process, a liquid penetrates the grain boundaries of the polycrystal, and this leads to their fragmentation, resulting in loss of the original particle shape. Subsequently, this fragmentation of particles leads to an increased mobility of single grains due to the liquid capillary force, and considerable shrinkage occurs [15, 16]. The process observed in this work is similar to the secondary rearrangement process reported by Petzow and Kaysser, but the fragmentation of Si_3N_4 particle in the solution–reprecipitation stage is not obvious. Detailed studies on the fragmentation of Si_3N_4 by a liquid are necessary.

The pore-elimination process by particle migration in the solution–reprecipitation stage has been ignored in most of the papers concerning the sintering of Si_3N_4 ceramics with an oxide additive, but in recent work is often discussed in the literature [12]. In this work, the particle-rearrangement process and the cooperative-flow process of a particle/liquid mixture in the solution–reprecipitation stage have been confirmed firstly in the shrinkage rate curve. These processes are considered to take place during the sintering of Si_3N_4 ceramics and solid solutions.

Densification at 1700–1950 °C proceeds accompanying the grain growth. Cao et al. [19] have investigated the change in mean grain size during the sintering of α′-sialon at 1400–1800 °C, and they reported that the mean grain size was almost constant at temperatures lower than 1600 °C, but increased from 1 μm to 3 μm at temperatures from 1600–1800 °C. Furthermore, Chatfield *et al.* [20] reported that the final products of α′-sialon frequency maintained a core of unreacted α-Si_3N_4 raw material in α′-sialon particles. Grain growth in the presence of a liquid has been interpreted in terms of Ostwald ripening by the solution–reprecipitation mechanism [21]. The difference in the structure between the core and the rim of α′-sialon particles, as reported by Chatfield *et al.*, can suggest the operation of the Ostwald ripening process. In the case of densification accompanying the grain growth, the mechanism of Ostwald ripening with shape accommodation has been proposed [15, 16]. In this sintering mechanism, the grains grow due to Ostwald ripening, and, subsequently, contact flattening occurs when large grains come into contact with other large ones. Then liquid becomes available in the space between the grains, and contributes to the densification by flowing into residual pores and also by facilitating the rearrangement of the grains [16]. In the present work, at 1800 °C, the grains, which were probably grown by an Ostwald ripening process, are observed, and they contact through the well-filled liquid bridge (Fig. 7e). At 1900 °C, the grains agglomerate (Fig. 7f), and seem to contact directly at the facets (indicated by white arrows), implying the occurrence of contact flattening. Furthermore, as seen in Fig. 7e and f, the size of pores in the specimen increases remarkably at 1800–1900 °C, which can be interpreted as the small pores becoming filled with liquid, and moving along the grain boundaries towards middle-size pores, subsequently forming large pores. The mechanism of Ostwald ripening with shape accommodation is anticipated to occur in this temperature range.

4.3. Influence of silica content and sialon formation on densification

It is known that the densification fraction that can be achieved through the rearrangement and viscous-flow processes depends on the volume fraction of liquid phase, because, after particle rearrangement, the residual pores can be filled with the liquid phase [9]. Table IV shows the amount of nitrides and oxides in the mixed powders, assuming that all the oxygen detected in the raw nitride powders forms SiO_2 for

TABLE IV Estimation of nitride and oxide content in the powder mixture

	Si_3N_4	AlN	Y_2O_3	SiO_2	Al_2O_3
Specimen S (wt %)	73.66	14.91	9.25	1.81	0.36
(vol %)	76.58	15.15	5.73	2.25	0.30
Specimen B (wt %)	74.33	14.91	9.25	1.14	0.36
(vol %)	77.38	15.18	5.71	1.42	0.30
Specimen C (wt %)	74.66	14.91	9.25	0.80	0.36
(vol %)	77.79	15.19	5.71	1.00	0.30
Specimen S1 (wt %)	73.29	14.84	9.20	2.30	0.35
(vol %)	76.08	15.08	5.67	2.88	0.29
Specimen S2 (wt %)	72.96	14.76	9.15	2.79	0.35
(vol %)	75.62	14.94	5.65	3.48	0.29

Si_3N_4 and Al_2O_3 for AlN, respectively. The silica, alumina and yttria will be a liquid phase before the formation of α′-sialon, and the amount of liquid phase is 8.28 vol% for specimen S, 7.43 vol % for specimen B, 7.01 vol % for specimen C, 8.84 vol % for specimen S1 and 9.42 vol % for specimen S2, respectively. Depending on the volume of liquid-phase, specimen S2 indicates a much larger amount of shrinkage in the samples.

In specimen S2, the formation of α′-sialon is observed at 1450 °C, and the shrinkage rate decreases rapidly at 1450–1500 °C. Therefore, the retardation of shrinkage rate is closely related to the formation of sialon. On the other hand, the influence of α′-sialon formation on densification cannot be found in specimens S, B and S1. This may be ascribed to the amount of liquid phase during sintering. In the presence of a large amount of liquid, the liquid-flow process contributes to the densification further, but is strongly influenced by the change in viscosity of the liquid. The densification at temperatures higher than 1300 °C is due to a liquid-flow process. As the ingredients of the liquid are incorporated into the α-structure during the formation of α′-sialon [3–5], the viscosity of the liquid become high. Hence, in the case of specimen S2 the retardation of the shrinkage rate due to the formation of α′-sialon is observed.

As seen in Table III, a fully densified specimen cannot be obtained in this work. Cao *et al.* [22] reported that densification of α′-sialon was accelerated with increasing oxygen content in the raw powders. They have also produced an almost densified specimen by sintering of raw Si_3N_4 powder with an oxygen content of about 2 wt % at 1900 °C. In its fractured surface the coarsening of grains was observed. These results reveal that particle rearrangement, cooperative flow of the particle/liquid mixture and, probably, Ostwald ripening processes, are active due to the rich oxygen content in the raw powder. Consequently, they could produce almost fully densified α′-sialon.

5. Conclusion

Densification of α′-sialon proceeds via liquid flow, particle rearrangement and cooperative flow of the particle/liquid mixture, as well as, probably, Ostwald ripening with shape accommodation in the solution–reprecipitation stage. The rearrangement and cooperative flow processes result in a large amount of shrinkage during sintering, but the liquid-flow process is retarded due to the formation of α′-sialon. In order to obtain fully densified sialon ceramics, it is useful to add silica to the raw materials.

References

1. Y. OYAMA and O. KAMIGAITO, *Jpn J. Appl. Phys.* **10** (1971) 1637.
2. K. H. JACK and W. I. WILSON, *Nature (Lond.) Phys. Sci.* **238** (1977) 28.
3. S. HAMPSHIRE, H. K. PARK, D. P. THOMPSON and K. H. JACK, *Nature* **274** (1978) 880.
4. Z.-K. HUANG and P.-S. YAN, *J. Mater. Sci.* **27** (1992) 5640.
5. K. ISHIZAWA, N. AYUZAWA, A. SHIRATANI, M. TAKAI, N. UCHIDA and M. MITOMO, in "Ceramics Materials and Components for Engines", edited by W. Bunk and H. Hausner (German Ceramics Society, Bad Honnef, FRG, 1986) pp. 511–18.
6. A. NAGEL, P. GREIL and G. PETZOW, *Rev. de Chem. Miner.* **22** (1985) 437.
7. S. SLASOR and D. P. THOMPSON, in "Non-Oxide Technical and Engineering Ceramics", edited by S. Hampshire (Elsevier, London, 1986) pp. 223–30.
8. O. ABE, *J. Mater. Sci.* **25** (1990) 3641.
9. W. D. KINGERY, *J. Appl. Phys.* **30** (1959) 301.
10. R. M. GERMAN "Liquid Phase Sintering" (Plenum Press, New York, 1985) Ch. 4F.
11. K. WATARI, M. E. BRITO, M. OHASHI and S. KANZAKI, *J. Am. Ceram. Soc.*, submitted.
12. D. SUTTOR and G. S. FISCHMAN, *ibid.* **75** (1992) 1063.
13. K. WATARI, S. KANZAKI, M. ASAYAMA, A. TSUGE, K. ISOZAKI and H. HIROTSURU, in "Proceedings of the Annual Meeting of The Ceramics Society of Japan", (Ceramics Society of Japan, Tokyo, 1993) p. 610.
14. W. D. KINGERY, in "Ceramics Fabrication Process", edited by W. D. Kingery (Wiley, New York, 1978) pp. 131–40.
15. G. PETZOW and W. A. KAYSSER, in "Sintered Metal-Ceramics Composite", edited by G. S. Upahyaya (Elsevier Science, Amsterdam, 1984) pp. 51–70.
16. G. PETZOW and W. A. KAYSSER, in "Sintering Key Papers", edited by S. Somiya and Y. Moriyoshi, (Elsevier Applied Science, London, New York, 1990) pp. 595–614.
17. D. N. YOON and W. J. HUPPMANN *Acta Metall.* **27** (1979) 693.
18. H. H. PARK, S.-J. CHO and D. N. YOON, *Metall. Trans.* **15A** (1984) 1075.
19. G. Z. CAO, R. METSELAAR and G. ZIEGLER, *J. Eur. Ceram. Soc.* **11** (1993) 115.
20. C. CHATFIELD, T. EKSTROM and M. MIKUS, *J. Mater. Sci.* **21** (1986) 2297.
21. L. S. SIGL and H-J. KLEEBE, *J. Am. Ceram. Soc.* **76** (1993) 773.
22. G. Z. CAO, R. METSELAAR and G. ZIEGLER, *J. Mater. Sci. Lett.* **11** (1992) 685.

Received 21 December 1993
and accepted 16 May 1994